Electronic Supplementary Information

Cu_xNi_y Alloy Nanoparticles Embedded in Nitrogen-Carbon Network for Efficient Conversion of Carbon Dioxide

Dongxing Tan[a], Jianling Zhang*[a], Xiuyan Cheng[a], Xiuniang Tan[a], Jinbiao Shi[a], Bingxing Zhang[a], Buxing Han[a], Lirong Zheng[b], and Jing Zhang[b]

[a]Beijing National Laboratory for Molecular Sciences, CAS Key Laboratory of Colloid, Interface and Chemical Thermodynamics, Institute of Chemistry, Chinese Academy of Sciences, School of Chemical Sciences, University of Chinese Academy of Sciences, Beijing 100049, P.R.China.

[b]Beijing Synchrotron Radiation Facility (BSRF), Institute of High Energy Physics, Chinese Academy of Sciences, Beijing 100049, P.R.China.

**Correspondence Email: zhangjl@iccas.ac.cn.*

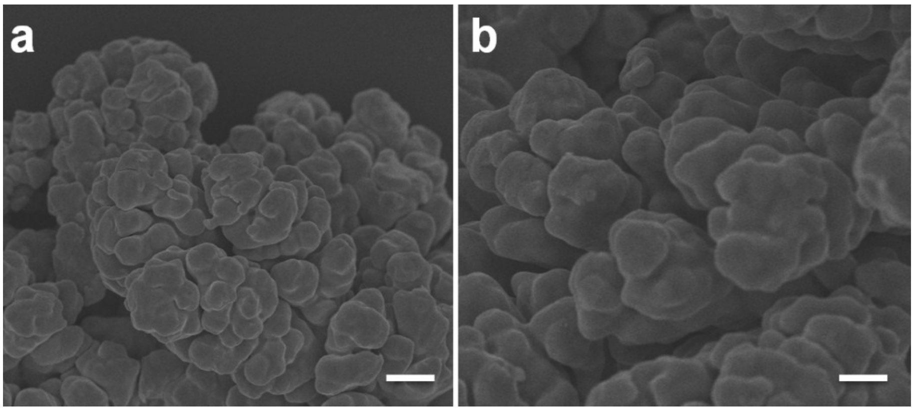

Fig.S1 SEM images of Cu powder. Scale bars, 5 um in (a), 2 um in (b).

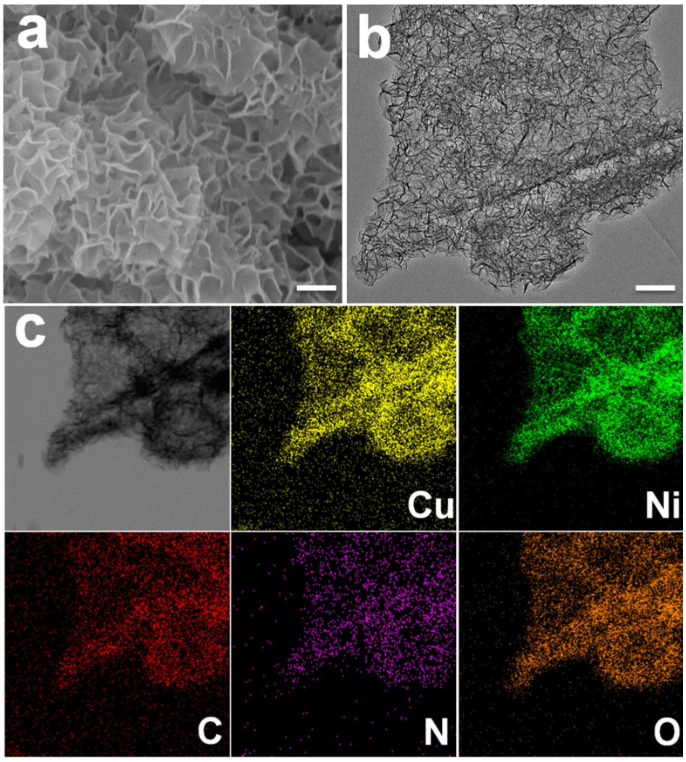

Fig. S2 SEM (a) and TEM images (b) and EDX mapping (c) of Cu/Ni bimetallic complex. Scale bars, 300 nm in (a), 100 nm in (b). The complex consists of copper, nickel, carbon, nitrogen and oxygen elements, and the elements are evenly distributed throughout the sample.

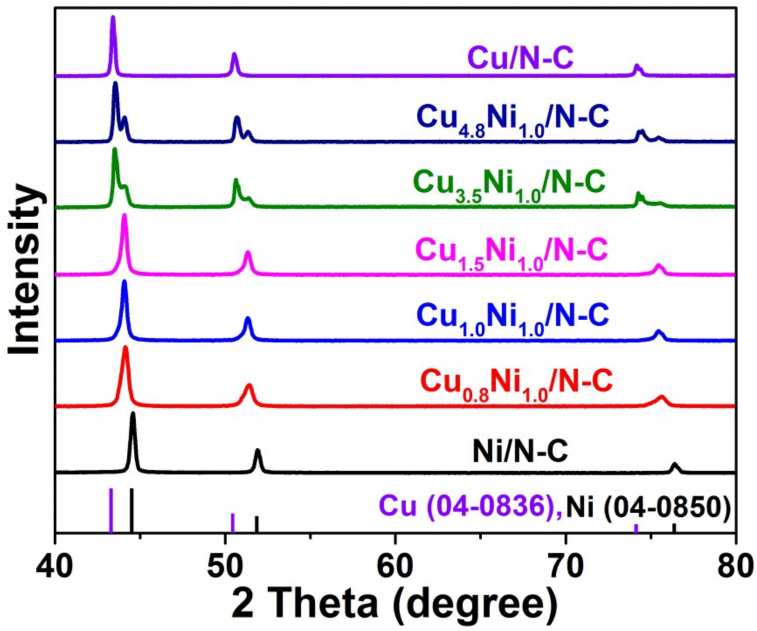

Fig. S3 XRD patterns of the Cu_xNi_y/N-C. The standard diffraction patterns for Cu (JCPDS no. 04-0836) and Ni (JCPDS no. 04-0850) are provided as references. For $Cu_{0.8}Ni_{1.0}$/N-C, $Cu_{1.0}Ni_{1.0}$/N-C and $Cu_{1.5}Ni_{1.0}$/N-C, the Cu_xNi_y nanoparticles exist as alloy, while for $Cu_{3.5}Ni_{1.0}$/N-C and $Cu_{4.8}Ni_{1.0}$/N-C, the Cu_xNi_y nanoparticles present as a mixture of metallic copper and Cu/Ni bimetallic alloys.

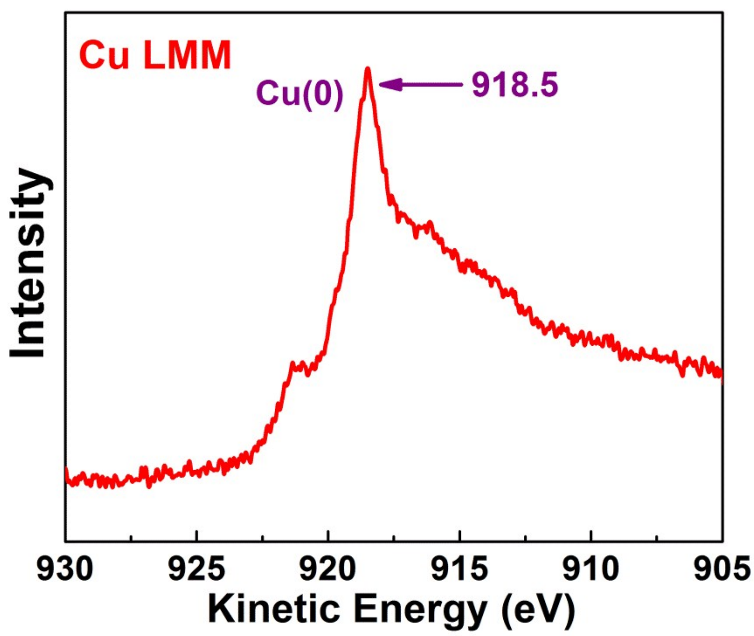

Fig. S4 The Auger Cu LMM spectrum of $Cu_{1.0}Ni_{1.0}$/N-C.

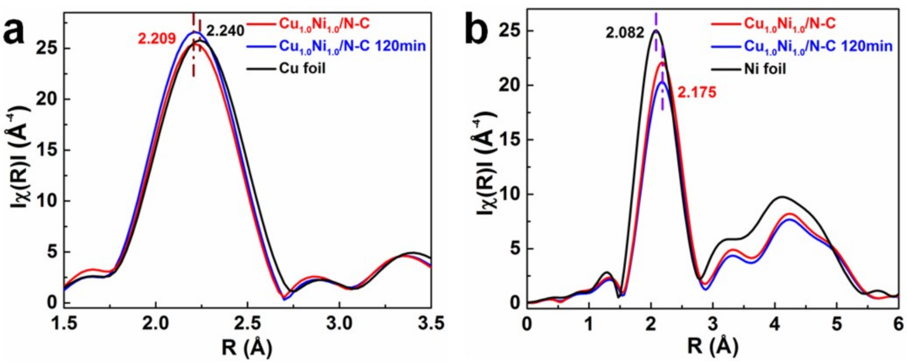

Fig. S5 K^3-weighted (K) function of the EXAFS spectra of $Cu_{1.0}Ni_{1.0}$/N-C, $Cu_{1.0}Ni_{1.0}$/N-C after electrolysis for 120 min, Cu foil and Ni foil.

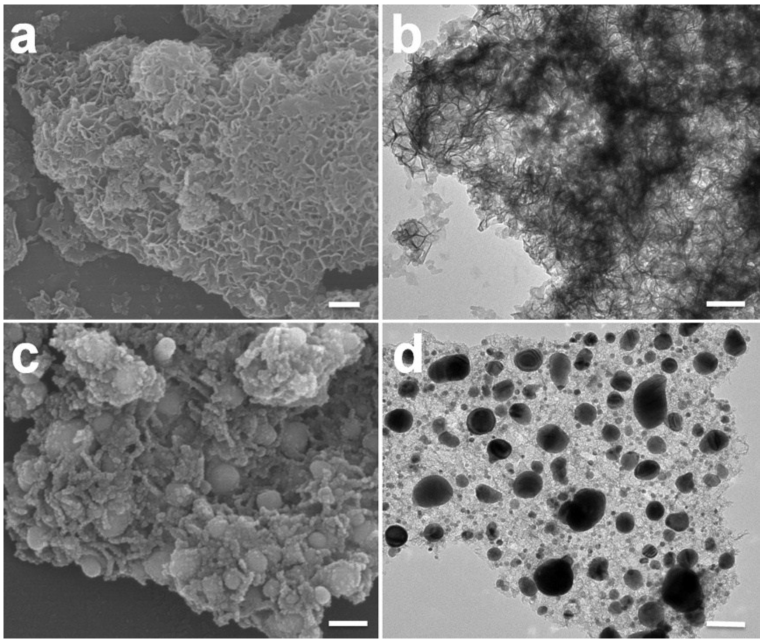

Fig. S6 SEM (a, c) and TEM (b, d) images of $Cu_{0.8}Ni_{1.0}$/N-C complex (a, b) and $Cu_{0.8}Ni_{1.0}$/N-C catalyst (c, d). Scale bars, 200 nm in (a), 100 nm in (b), 100 nm in (c), 100 nm in (d).

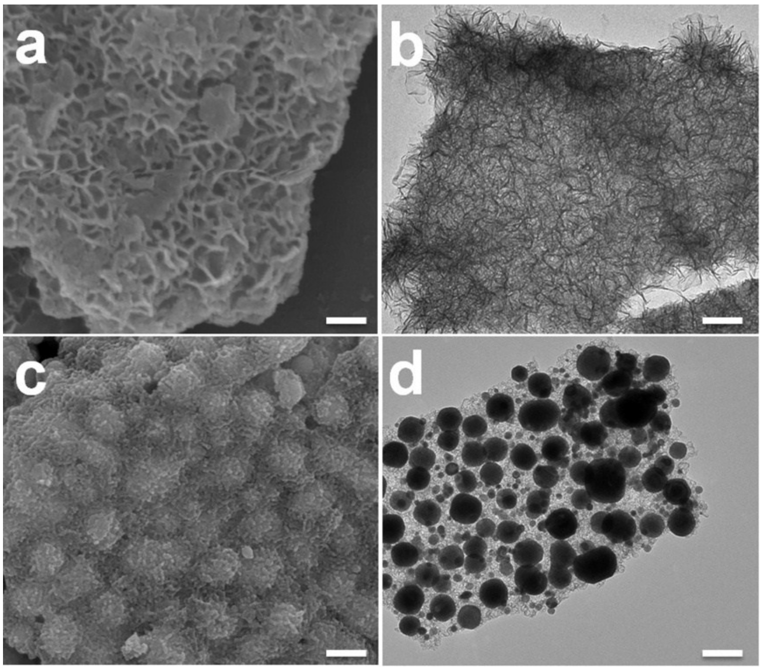

Fig. S7 SEM (a, c) and TEM (b, d) images of $Cu_{1.5}Ni_{1.0}$/N-C complex (a, b) and $Cu_{1.5}Ni_{1.0}$/N-C catalyst (c, d). Scale bars, 100 nm in (a), 100 nm in (b), 100 nm in (c), 200 nm in (d).

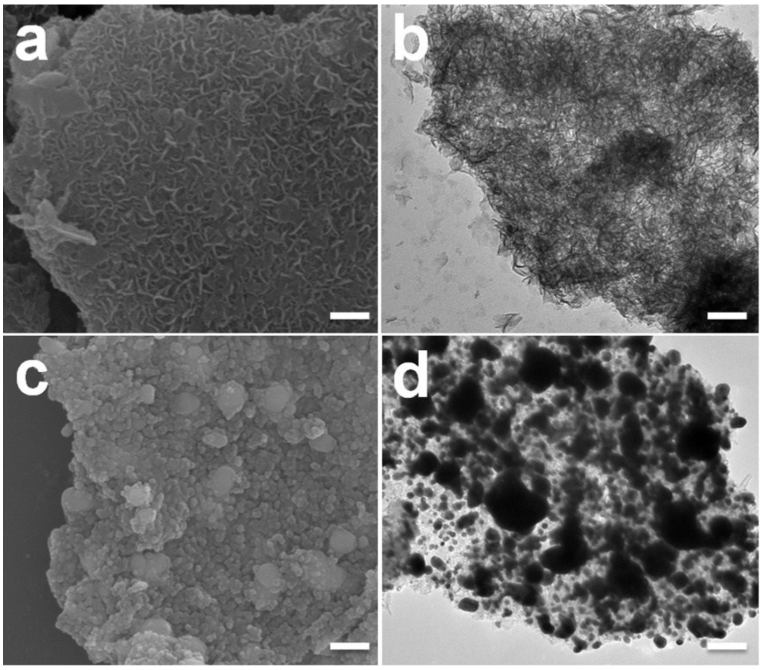

Fig. S8 SEM (a, c) and TEM (b, d) images of $Cu_{3.5}Ni_{1.0}$/N-C complex (a, b) and $Cu_{3.5}Ni_{1.0}$/N-C catalyst (c, d).Scale bars, 200 nm in (a), 100 nm in (b), 100 nm in (c), 200 nm in (d).

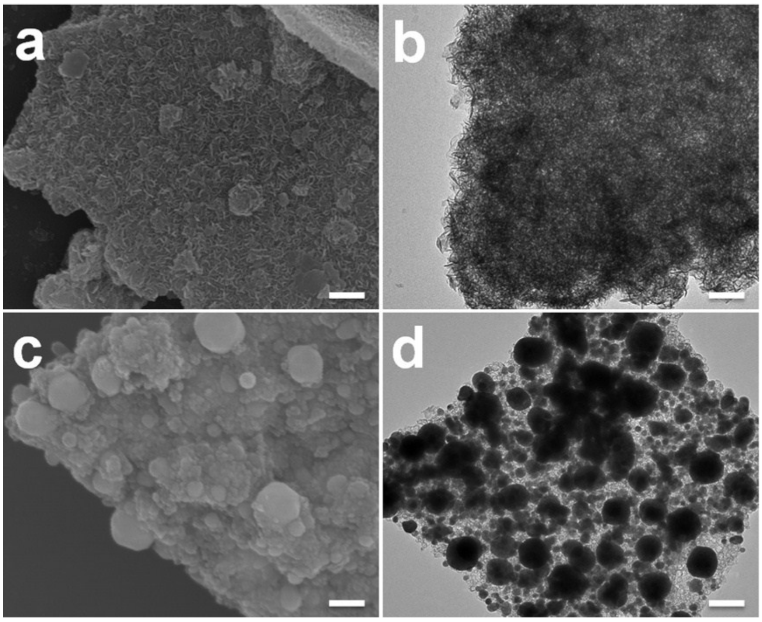

Fig. S9 SEM (a, c) and TEM (b, d) images of $Cu_{4.8}Ni_{1.0}$/N-C complex (a, b) and $Cu_{4.8}Ni_{1.0}$/N-C catalyst (c, d).Scale bars, 200 nm in (a), 100 nm in (b), 100 nm in (c), 100 nm in (d).

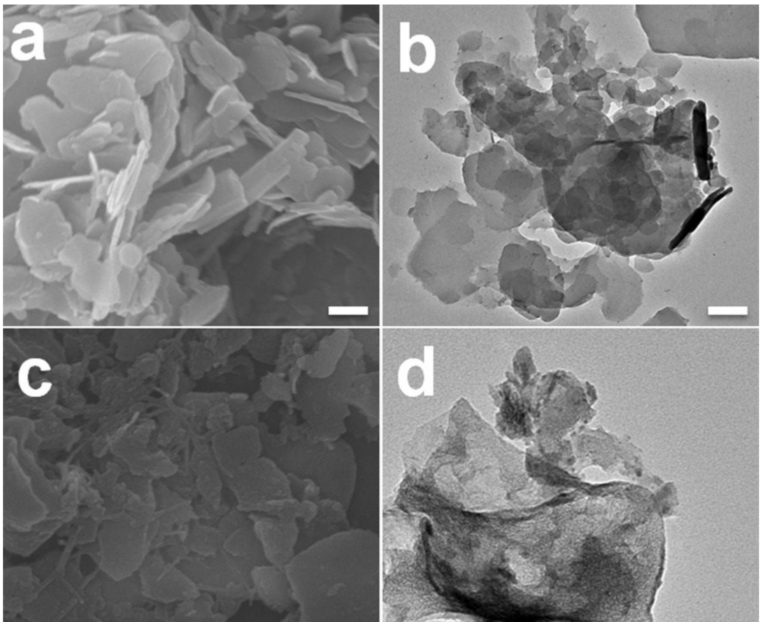

Fig. S10 SEM (a, c) and TEM (b, d) images of Cu/N-C complex (a, b) and Cu/N-C catalyst (c, d). Scale bars, 200 nm in (a), 100 nm in (b), 200 nm in (c), 100 nm in (d).

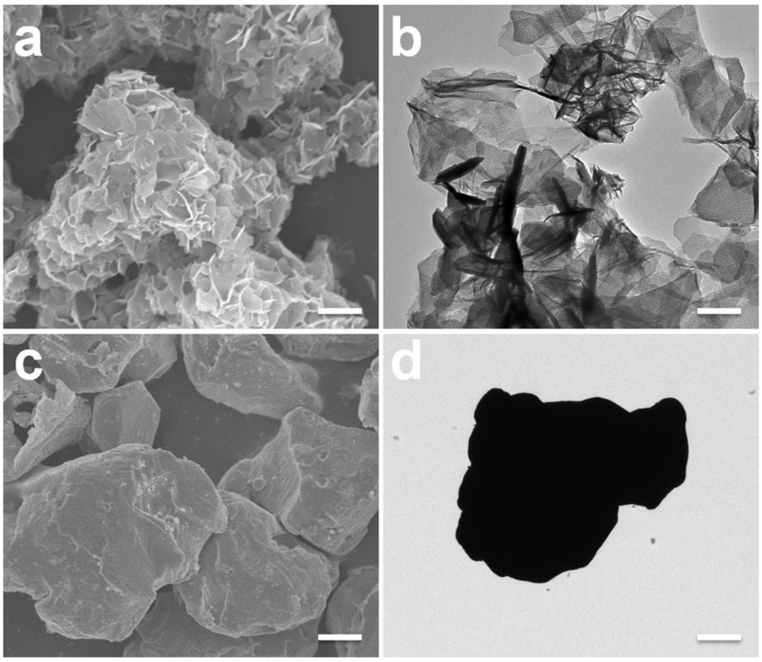

Fig. S11 SEM (a, c) and TEM (b, d) images of Ni/N-C complex (a, b) and Ni/N-C catalyst (c, d). Scale bars, 100 nm in (a), 200 nm in (b), 500 nm in (c), 3 um in (d).

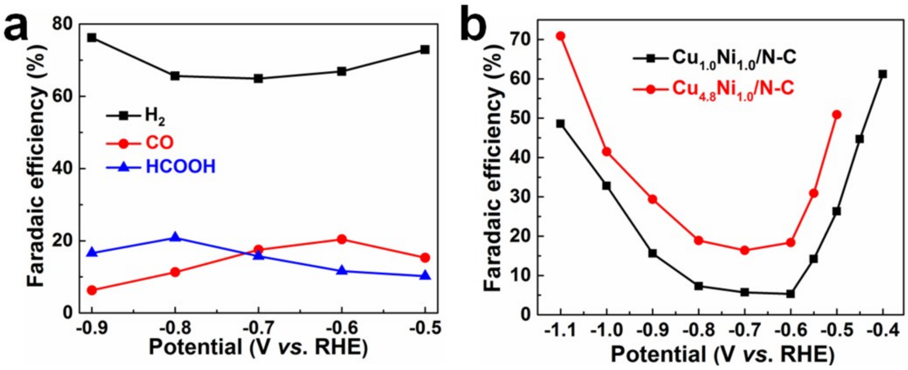

Fig. S12 Faradaic efficiency of H_2, CO and HCOOH at various potentials for Cu/N-C (a). Faradaic efficiency of H_2 at various potentials for $Cu_{1.0}Ni_{1.0}$/N-C and $Cu_{4.8}Ni_{1.0}$/N-C (b).

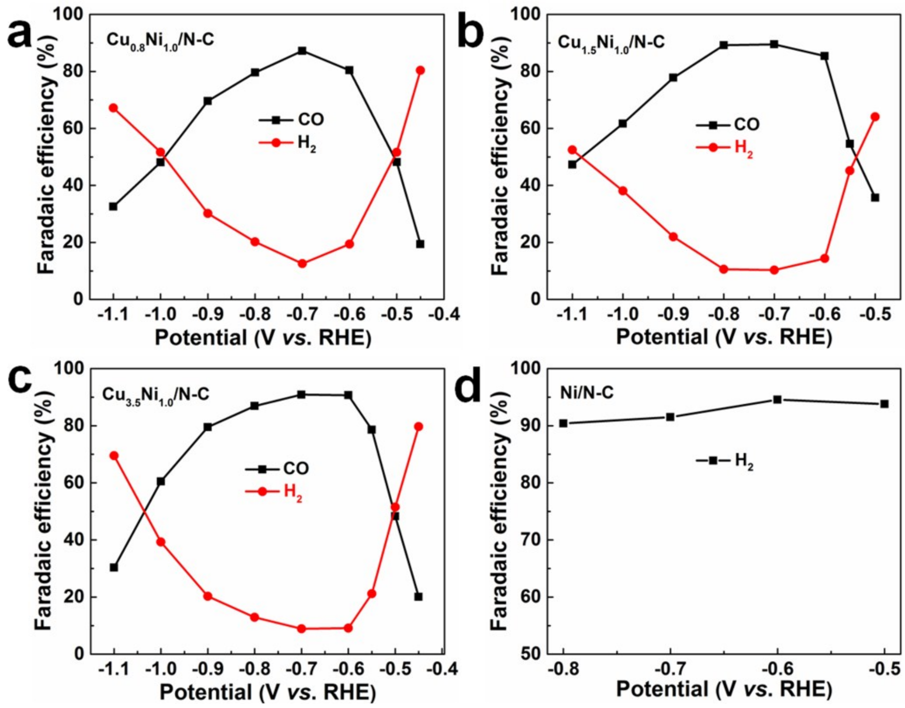

Fig. S13 Faradaic efficiency of H_2 and CO at various potentials for $Cu_{0.8}Ni_{1.0}$/N-C (a), $Cu_{1.5}Ni_{1.0}$/N-C (b) and $Cu_{3.5}Ni_{1.0}$/N-C (c). Faradaic efficiency of H_2 at various potentials for Ni/N-C (d).

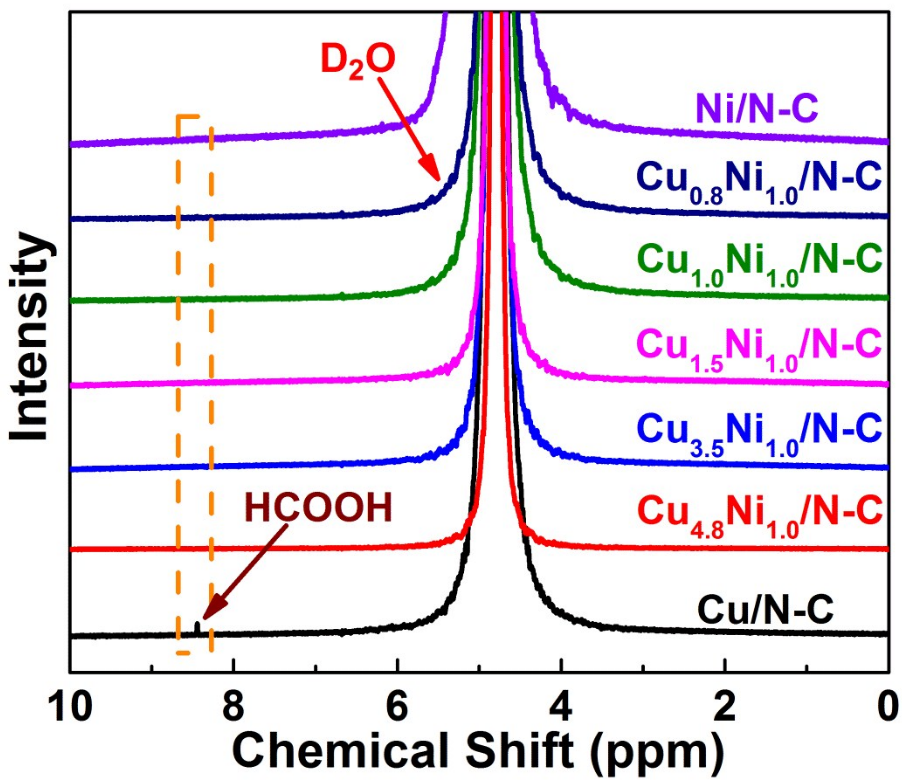

Fig. S14 ^1H NMR spectra of the electrolytes after CO_2 reduction at different potentials versus RHE.

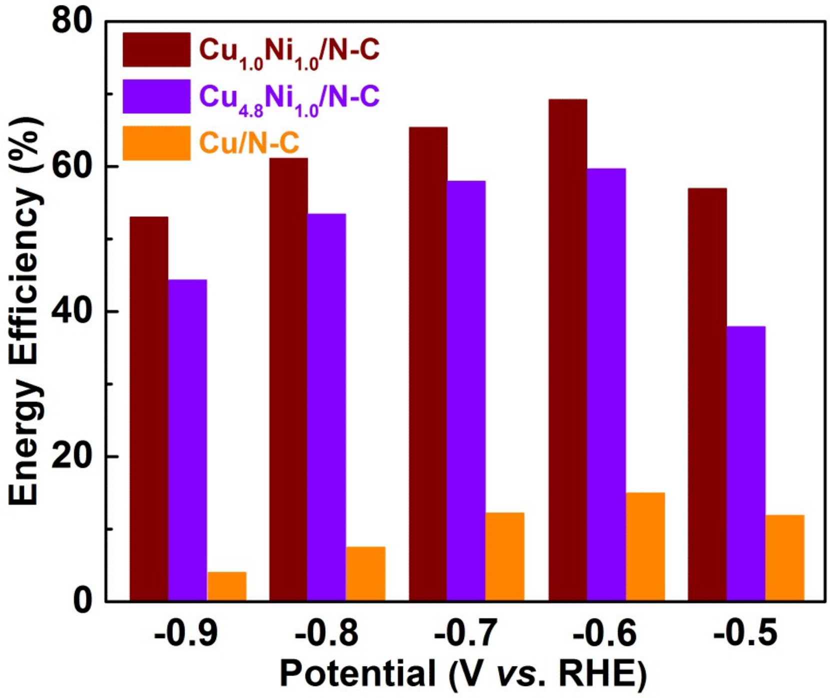

Fig. S15 Energy efficiency of CO formation over different catalysts at different applied potentials.

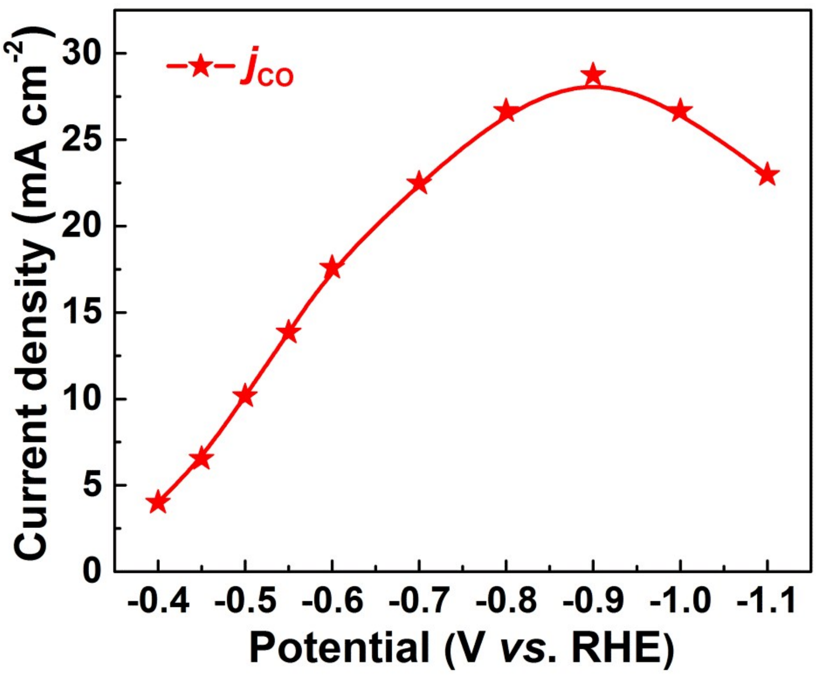

Fig. S16 Partial current density of $Cu_{1.0}Ni_{1.0}$/N-C at the applied potentials.

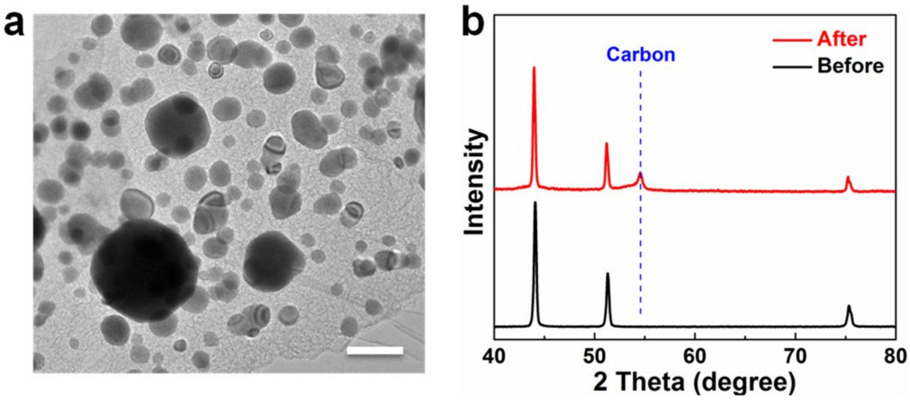

Fig. S17 TEM image (a) and XRD patterns (b) of $Cu_{1.0}Ni_{1.0}$/N-C after CO_2 reduction at -0.61 V for 38 h. Scale bars: 100 nm in (a).

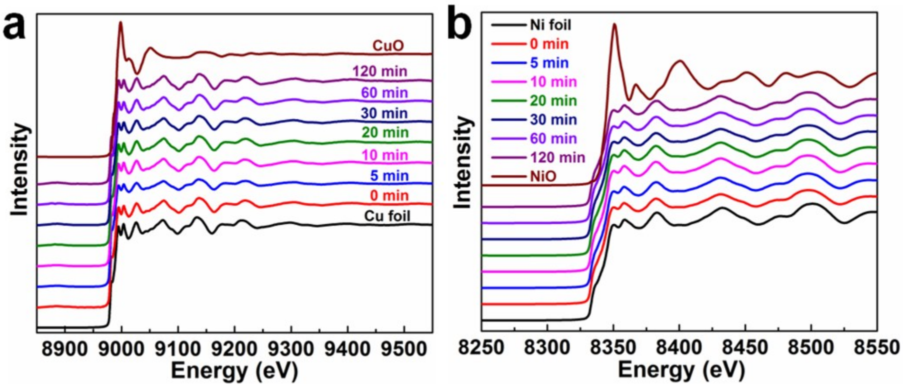

Fig. S18 Cu (a) and Ni (b) K-edge XANES spectra of $Cu_{1.0}Ni_{1.0}$/N-C and $Cu_{1.0}Ni_{1.0}$/N-C after different electrolytic time. Cu foil, CuO, Ni foil and NiO were used as contrast samples.

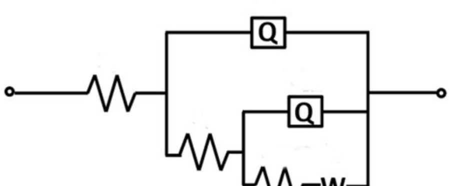

Fig. S19 The electrical equivalent circuit used for simulating the experimental impedance data.

Table S1. Element contents in Cu_xNi_y/N-C electrocatalysts as well as the molar ratios of Cu to Ni.

electrocatalysts	Cu (wt%)	Ni (wt%)	C (wt%)	N (wt%)	O (wt%)	Molar ratio of Cu : Ni
Cu/N-C	80.1	/	13.4	5.0	1.5	/
$Cu_{0.8}Ni_{1.0}$/N-C	31.9	36.4	25.0	4.6	2.1	0.8:1.0
$Cu_{1.0}Ni_{1.0}$/N-C	37.8	33.5	23.2	4.2	1.3	1.0:1.0
$Cu_{1.5}Ni_{1.0}$/N-C	43.1	27.9	25.0	3.1	0.9	1.5:1.0
$Cu_{3.5}Ni_{1.0}$/N-C	60.3	16.1	17.2	5.1	1.3	3.5:1.0
$Cu_{4.9}Ni_{1.0}$/N-C	64.9	12.4	18.5	2.3	1.9	4.8:1.0
Ni/N-C	/	94.1	3.5	1.1	1.3	/

Table S2. The catalytic performances of Cu-based alloys and bimetallic catalysts.

Catalyst	Electrolyte	Product	FE(CO)	Potential	Current density	Ref.
$Pd_{85}Cu_{15}/C$	0.1 M $KHCO_3$	CO	86%	-0.89	6.9	1
C-Cu/SnO_2-0.8	0.5 M $KHCO_3$	CO, HCOOH	93%	-0.70	4.6	2
$CuInO_2$	0.1 M $KHCO_3$	CO,HCOOH	20%	-0.60	2.3	3
Cu-In alloy	0.1 M $KHCO_3$	CO, HCOOH	70%	-0.80	/	4
Cu-Sn	0.1 M $KHCO_3$	CO, HCOOH	90%	-0.60	1.0	5
o-AuCu NP	0.1 M $KHCO_3$	CO, HCOOH	80%	-0.77	1.8	6
Cu-Pd (ordered)	1 M KOH	CO,CH_4, C_2H_4, C_2H_5OH	80%	-0.55	/	7
Cu-In	0.1 M $KHCO_3$	CO, HCOOH	85%	-0.60	0.7	8
FL-Pd_3Cu	0.1 M $KHCO_3$	CO	82.1%	-0.9	6.0	9
Cu/$Ni(OH)_2$	0.5 M $NaHCO_3$	CO	92%	-0.5	4.3	10
Cu-Pd-0.3	0.5 M $KHCO_3$	CO	93%	-0.87	5.5	11
CuIn20	0.1 M $KHCO_3$	CO, HCOOH	93%	-0.60	2	12
Mesoporous Pd_7Cu_3	0.1 M $KHCO_3$	CO	80%	-0.80	2	13
$Cu_{16}Ag_{84}$ dendrite	0.5 M $KHCO_3$	CO	45%	-0.87	/	14
Ag–Cu core–shell	0.1 M $KHCO_3$	CO, CH_4, C_2H_4	82%	-1.06	1.8	15
Au-coated Cu NW	0.5 M $KHCO_3$	CO	33%	-0.65	13.5	16
$Cu_{87}Sn_{13}$	0.1 M $KHCO_3$	CO, HCOOH, CH_4, C_2H_4	60%	-1.0	/	17
$Cu_{1.0}Ni_{1.0}$/N-C	0.5 M $KHCO_3$	CO	94.5%	-0.60	18.8	This work

References

1 Z. Yin, D. Gao, S. Yao, B. Zhao, F. Cai, L. Lin, P. Tang, P. Zhai, G. Wang and D. Ma, *Nano Energy*, 2016, **27**, 35-43.

2 Q. Li, J. Fu, W. Zhu, Z. Chen, B. Shen, L. Wu, Z. Xi, T. Wang, G. Lu and J. J. Zhu, *J. Am. Chem. Soc.*, 2017, **139**, 4290-4293.

3 G. O. Larrazábal, A. J. Martín, S. Mitchell, R. Hauert and J. Pérezramírez, *ACS Catal.*, 2016, **6**, 6265-6274.

4 A. Jedidi, S. Rasul, D. Masih, L. Cavallo and K. Takanabe, *J. Mater. Chem. A*, 2015, **3**, 19085-19092.

5 S. Sarfraz, A. T. Garciaesparza, A. Jedidi, L. Cavallo and K. Takanabe, *ACS Catal.*, 2016, **6**, 2842-2851.

6 D. Kim, C. Xie, N. Becknell, Y. Yu, M. Karamad, K. Chan, E. J. Crumlin, J. K. Norskov and P. Yang, *J. Am. Chem. Soc.*, 2017, **139**, 8329-8336.

7 S. Ma, M. Sadakiyo, M. Heima, R. Luo, R. T. Haasch, J. I. Gold, M. Yamauchi and P. J. Kenis, *J. Am. Chem. Soc.*, 201**6**, **139**, 47-50.

8 S. Rasul, D. H. Anjum, A. Jedidi, Y. Minenkov, L. Cavallo and K. Takanabe, *Angew. Chem., Int. Ed.*, 2015, **54**, 2146-2150.

9 W. Zhu, L. Zhang, P. Yang, X. Chang, H. Dong, A. Li, C. Hu, Z. Huang, Z. J. Zhao and J. Gong, *Small*, 2017, **14**, 1703314.

10 L. Dai, Q. Qin, P. Wang, X. Zhao, C. Hu, P. Liu, R. Qin, M. Chen, D. Ou and C. Xu, *Sci. Adv.*, 2017, **3**, e1701069.

11 D. Chen, Q. Yao, P. Cui, H. Liu, J. Xie and J. Yang, *ACS Appl. Energy Mater.*, 2018, **1**, 883-890.

12 W. Luo, W. Xie, R. Mutschler, E. Oveisi, G. L. De Gregorio, R. Buonsanti and A. Züttel, *ACS Catal.*, 2018, **8**, 6571-6581.

13 M. Li, J. Wang, P. Li, K. Chang, C. Li, T. Wang, B. Jiang, H. Zhang, H. Liu and Y. Yamauchi, *J. Mater. Chem. A*, 2016, **4**, 4776-4782.

14 J. Choi, M. J. Kim, H. A. Sang, I. Choi, J. H. Jang, S. H. Yu, J. J. Kim and S. K. Kim, *Chem. Eng. J.*, 2016, **299**, 37-44.

15 Z. Chang, S. J. Huo, Z. Wei, J. Fang and H. Wang, *J. Phys. Chem. C*, 2017*,* **121***,* 11368-11379.

16 K. Chen, X. Zhang, T. Williams, L. Bourgeois and D. R. Macfarlane, *Electrochim. Acta*, 2017, **239**, 84-89.

17 M. Morimoto, Y. Takatsuji, R. Yamasaki, H. Hashimoto, I. Nakata, T. Sakakura and T. Haruyama, *Electrocatalysis,* 2017, **9**, 1-10.